DOI: 10.1021/ma101723y

Macromolecules
ARTICLE

High Intensity Response of Photopolymer Materials for Holographic Grating Formation

Shui Liu, Michael R. Gleeson, Jinxin Guo, and John T. Sheridan*

School of Electrical, Electronic and Mechanical Engineering, Communication and Optoelectronic Research Centre, The SFI-Strategic Research Cluster in Solar Energy Conversion, College of Engineering, Mathematical and Physical Sciences, University College Dublin, Belfield, Dublin 4, Ireland

Received July 29, 2010; Revised Manuscript Received September 24, 2010

ABSTRACT: In order to further develop the understanding of photopolymer materials, a more complete physical model has become necessary. In particular, a more accurate description of the photochemical mechanisms occurring during the photopolymerization processes is needed. Generally, in photopolymers, the photosensitizer absorbs light of an appropriate wavelength, becoming excited and causing the production of primary radicals, R$^\bullet$. In free radical polymerization systems, the generation of R$^\bullet$ is a key factor in determining how much monomer is polymerized. This in turn is closely related to the refractive index modulation formed during holographic recording. In this article, we incorporate a detailed photoinitiation model into the nonlocal photopolymerization driven diffusion (NPDD) model. This model describes the following: (1) Photon absorption behavior and primary radical generation during *initiation*; (2) nonlocal macro-radical chain growth through *propagation*; (3) oxygen diffusion and replenishment for *inhibition*; (4) multiple *termination* mechanisms. This extended model is experimentally validated for high intensity holographic exposures to a polyvinylalcohol/acrylamide based photopolymer material.

1. Introduction

Photopolymer materials have received considerable attention in the literature, with applications in areas such as holographic data storage, hybrid optoelectronics, photo embossing, refractive and diffractive optical elements, and the self-trapping of light.[1−4] Such materials can record low loss, environmentally stable, and high contrast refractive index patterns, and they are relatively easy and inexpensive to fabricate and use. To further develop the functionality of these photopolymers, theoretical models and detailed material characterization are necessary in order to optimize material compositions and performance.

Previously,[5,6] extensive holographic exposure based studies have been presented to model the photochemical kinetics which take place during the photoinitiation processes. The aim was to precisely predict the number of photons that are absorbed by the photosensitizer, which results in the generation of primary radicals, R$^\bullet$. In this way, the initiation of photopolymer chains can be more accurately quantified. In this work, for the first time a much more detailed photoinitiation model is incorporated into the nonlocal photopolymerization driven diffusion (NPDD) model.[7−9] This significantly improves the model by taking account of the spatial and temporal effects associated with (1) photon absorption, regeneration or recovery of absorptive photosensitizer, and photosensitizer bleaching; (2) a more exact description of primary radical generation and removal; (3) nonlocal chain growth with nonsteady state kinetics, which leads to an quantitative explanation of polymerization rate, R_p; (4) simultaneous primary termination and bimolecular termination; (5) a more accurate representation of the generation of polymer chains; and (6) multiple inhibition effects. Therefore, a more accurate prediction for the formation of the recorded holographic gratings in a polyvinylalcohol/acrylamide (PVA/AA)[5−10] photopolymer material can be obtained.

Optimizing the photopolymerization processes requires that an appropriate exposure energy be delivered to the photopolymer material. This is because the induced photochemical kinetics depend on how the exposure energy is delivered. A recent study[9] has been carried out to investigate primary radical generation and inhibition effects in a PVA/AA photopolymer material, during and postholographic exposure, for relatively low intensity exposures, i.e., 0.05 mW/cm^2 ≤ I_0 ≤ 0.2 mW/cm^2. We now examine the intensity response of the same photopolymer material, when higher holographic exposure intensities are applied, i.e., 10 mW/cm^2 ≤ I_0 ≤ 150 mW/cm^2.

This article is organized as follows: In section 2, we thoroughly review the photochemical reactions that take place during and postholographic recording. The corresponding rate equations which govern each associated chemical species concentration are then derived, including both temporal and spatial effects. In section 3, the predictions of the model are examined by performing simulations for a variety of kinetic parameter values. In section 4, the volume fraction analysis is presented, which summarizes the temporal evolution of the grating refractive index modulation formed. The resulting complete NPDD model is then applied to simultaneously fit experimentally obtained transmission curves, growth and decay curves of refractive index modulation for a range of high intensity exposures. Kinetic parameter values are then determined using the model which optimally fits the experimental data. Finally, conclusions and discussions are presented in section 5.

2. Photochemical Kinetics

2.1. Initiation. During holographic exposure of a PVA/AA photopolymer material, when the photosensitizer is illuminated with light of a suitable wavelength, the ground state dye molecules, Dye, absorb photons of light and are promoted to a singlet excited state,[5,6] ^{1}Dye*, which can then be promoted through *intersystem crossing* into a more stable and longer lived triplet state, ^{3}Dye*. Both the excited singlet dye, and triplet dye molecules can return to their ground state, by multiple reactions, such as radiationless energy transfer, molecular collisions, fluorescence, inhibition effects etc.,[5,6] at the overall recovery rates r_1 (s^{-1}), r_2 (s^{-1}) respectively. Primary radicals, R$^\bullet$ (or ED$^\bullet$), and hydro dye radicals, HDye$^\bullet$, are generated when ^{3}Dye* reacts with the co-initiator ED, i.e., electron donor [triethanolamine

*Corresponding author. E-mail: john.sheridan@ucd.ie. Telephone: +353-1-716-1927. Fax: +353-1-283-0921.

 Published on Web 10/26/2010

(TEA), $C_6H_{15}NO_3$].[5,6] $R^\bullet$ further reacts with $HDye^\bullet$ causing the formation of an intermediate state of electron donor, ED_{int}, and the major bleached dye state, dihydro dye, H_2Dye.[5,6] Leuco Dye is also formed when $^3Dye^*$ reacts with the inhibitor, i.e., initially dissolved molecular oxygen.[5,6] These reactions can be summarized as follows,

$$Dye + h\nu \xrightarrow{k_a} {}^1Dye^* \tag{1.1}$$

$${}^1Dye^* \xrightarrow{r_1} Dye \tag{1.2}$$

$${}^1Dye^* \xrightarrow{k_{st}} {}^3Dye^* \tag{1.3}$$

$${}^3Dye^* + ED \xrightarrow{k_d} R^\bullet \text{ (or } ED^\bullet) + HDye^\bullet \xrightarrow{k_b} ED_{int} + H_2Dye \tag{1.4}$$

$${}^3Dye^* + Z \xrightarrow{k_z} \text{Leuco Dye} \tag{1.5}$$

$${}^3Dye^* \xrightarrow{r_2} Dye \tag{1.6}$$

where k_a (s^{-1}) is the rate of production of excited state photosensitizer, k_{st} (s^{-1}) is the intersystem crossing rate from $^1Dye^*$ to $^3Dye^*$,[6] k_d (cm^3/mol s) is the rate constant of electron donation with which ED becomes a free radical, $R^\bullet$ (or $ED^\bullet$), k_z (cm^3/mol s) is the inhibition rate constant associated with the reaction of oxygen with excited triplet dye molecules, i.e., formation of Leuco Dye, and k_b (cm^3/mol s) is the rate constant of the photobleaching process, i.e., formation of dihydro dye, H_2Dye.

When a photopolymer layer is exposed with a sinusoidal spatial irradiance distribution, a grating is formed by the repeated bright (illuminated) and dark (unilluminated) periodic fringe pattern, thus the spatial variations need to be taken into account when modeling the dye kinetics. Using the chemical reactions described, in eqs 1.1−1.6, a set of first order coupled differential rate equations, which govern the evolution of the photosensitizer concentrations, [Dye, $^1Dye^*$ $^3Dye^*$, and $HDye^\bullet$] in space, x, and time, t, can be given as follows:

$$\frac{d[Dye(x,t)]}{dt} = -k_a[Dye(x,t)] + r_1[{}^1Dye^*(x,t)] + r_2[{}^3Dye^*(x,t)] \tag{2}$$

$$\frac{d[{}^1Dye^*(x,t)]}{dt} = k_a[Dye(x,t)] - r_1[{}^1Dye^*(x,t)] - k_{st}[{}^1Dye^*(x,t)] \tag{3}$$

$$\frac{d[{}^3Dye^*(x,t)]}{dt} = k_{st}[{}^1Dye^*(x,t)] - r_2[{}^3Dye^*(x,t)] - k_z[{}^3Dye^*(x,t)][Z(x,t)] - k_d[{}^3Dye^*(x,t)][ED(x,t)] \tag{4}$$

$$\frac{d[HDye^\bullet(x,t)]}{dt} = k_d[{}^3Dye^*(x,t)][ED(x,t)] - k_b[HDye^\bullet(x,t)][ED^\bullet(x,t)] \tag{5}$$

A flowchart presented in ref 6 also succinctly summarizes the dye kinetics described above.

The spatially distributed irradiance is assumed to be purely cosinusoidal, thus the incident intensity can be expressed as, $I(x,t) = I_0'[1 + V\cos(Kx)]$, where V is the fringe visibility and $K = 2\pi/\Lambda$, with Λ representing the grating period. However, the incident intensity I_0 (mW/cm^2) must first be converted into the appropriate units (Einstein/cm^2s) using the formula,

$$I_0' = \frac{I_0 T_{sf} B}{d}\left(\frac{\lambda}{N_a hc}\right)$$

where λ (nm) is the wavelength of the incident light, N_a (mol^{-1}) is Avogadro's constant, c (m/s) is the speed of light, h (J s) is Plank's constant, and T_{sf} is a correction factor to account for scattering losses, T_s, and Fresnel losses T_f.[10] $B = 1 - \exp(-\varepsilon[A_0]d)$, is an absorptive fraction which determines a material layer's initial absorptive capacity and is a function of the initial photosensitizer concentration, $[A_0]$ (mol/cm^3), the molar absorptivity, ε (cm^2/mol), and the material layer thickness, d (cm). In this case, the rate of production of the excited state photosensitizer, appearing in eqs 2 and 3, can be represented by $k_a = \phi\varepsilon d I_0'$ (s^{-1}),[9] where ϕ (mol/Einstein) is the quantum yield[10] of the reaction.

The central mechanism in the initiation stage is the production of primary radicals, $R^\bullet$, (or $ED^\bullet$), which can undergo *three main processes*:

(1) Reacting with the monomer, **M** (in the local bright fringes and which subsequently diffuses in from the dark regions). This produces a chain initiating species, a monomer-radical, $M_1^\bullet$, i.e., the start of a photopolymer chain which has a chain length of one unit.[7−9,11] This reaction takes place involving the primary radical uses its own unpaired electron and a π electron from the C=C bond of the monomer molecule. This leaves one of the carbons with an unpaired electron. In this way, it becomes a monomer radical with an active tip.

(2) Scavenging. This takes place when the generated primary radicals react with inhibitor molecules to produce inactive or dead molecules,[5−10] i.e., ED_{dead}.

(3) Terminating the active growing polymer chains. This is referred to as *primary termination*,[7−9,12] which is discussed in more detail in subsection 2.4.

The rate equations governing the concentrations of ED and $R^\bullet$ are,

$$\frac{d[ED(x,t)]}{dt} = -k_d[{}^3Dye^*(x,t)][ED(x,t)] \tag{6}$$

$$\frac{d[R^\bullet(x,t)]}{dt} = k_d[{}^3Dye^*(x,t)][ED(x,t)] - k_i[R^\bullet(x,t)][M(x,t)] - k_z[Z(x,t)][R^\bullet(x,t)] - k_{tp}[R^\bullet(x,t)][M^\bullet(x,t)] \tag{7}$$

where $[M(x,t)]$, $[M^\bullet(x,t)]$ and $[Z(x,t)]$ represent the concentrations of monomer, macro-radical (i.e., active growing polymer chain of chain length greater than and equal to one), and inhibitor, respectively. k_z (cm^3/mol s) is also the scavenging rate constant, where in this case we assume any reactions, i.e., with $^3Dye^*$, $R^\bullet$, $M^\bullet$, caused by the inhibitor molecules have the same reactivity; k_i (cm^3/mol s) and k_{tp} (cm^3/mol s) are the rate constants of initiation and primary termination, respectively.

2.2. Propagation. The monomer-radical, $M_1^\bullet$, will attach itself to a monomer, **M**, by addition to the C=C bond yielding another monomer radical with an active tip. This reaction takes place in the same way as the primary radical attaches to the monomer while generating $M_1^\bullet$. Then the

polymer chain grows by repeating this same step, which is referred to as chain propagation,

$$M_1^{\bullet} + \underbrace{M... + M... + M...}_{n} \xrightarrow{k_p} M_n^{\bullet}, \tag{8}$$

where $M_n^{\bullet}$ represents a macro-radical made up of n monomeric units ($n \geq 1$); and k_p (cm^3/mol s) is the rate constant of propagation. In this model, no distinction is made between the different steps made as each monomeric unit is attached.[7−9,12−14] Simultaneously, the macro-radicals are also undergoing the following reactions:

(1) The growing macro-radical can involve chain transfer[14] to another monomer molecule at the rate constant k_{tr}, producing a terminated polymer chain, M_n, and freeing the originally attached primary radical, $R^{\bullet}$, i.e., regeneration.
(2) Besides the primary termination mechanism, the macro-radicals produced can also terminate one another. This secondary termination mechanism is referred as to *bimolecular termination*,[7−9,13,14] and is discussed in more details in subsection 2.4.
(3) Similar to the primary radicals, the macro-radicals can also be scavenged by the inhibitor molecules. This is assumed to take place at the same rate constant of inhibition, k_z.

In some of the previous models,[15−18] it was assumed that under the steady state condition the rate of macro-radical concentration is constant, i.e.,

$$\frac{d[M^{\bullet}(x,t)]}{dt} = 0$$

Making this assumption permits an analytic solution for $[M^{\bullet}(x,t)]$, and hence the polymerization rate,[16,17] R_p (s^{-1}), to be derived by,

$$R_p = k_p[M^{\bullet}(x,t)][M(x,t)] = k_p \frac{\sqrt{8k_tR_i(x,t) + k_z^2[Z(x,t)]^2} - k_z[Z(x,t)]}{4k_t}[M(x,t)] \tag{9}$$

where $R_i(x,t) = 2\Phi I_a(x,t)$ is the initiation rate for an initiator quantum efficiency Φ, which is defined as the number of pairs of primary radicals generated per photon absorbed,[17] and I_a is the absorbed intensity.[17] However, when examining the high intensity response, large transient initiator concentrations, $[R^{\bullet}]$, will be produced.[19] Furthermore, during photopolymerization, the time varying viscosity effects (due to densification and cross-linking), which hinder molecule movement will become more pronounced.[7−9,12] Consequently, the dependence of the polymerization rate, R_p, on the initiation rate, R_i, will drop below that indicated by the square root relationship between R_p and R_i,[7,9,19] described in eq 9. Therefore, in this case, the steady state assumption is no longer valid, i.e.,

$$\frac{d[M^{\bullet}(x,t)]}{dt} \neq 0$$

and the macro-radical concentration must be represented in a more physically dynamic way, based on the chemical reactions taking place:

$$\frac{d[M^{\bullet}(x,t)]}{dt} = k_i[R^{\bullet}(x,t)][M(x,t)] - k_z[Z(x,t)][M^{\bullet}(x,t)] - k_{tr}[M^{\bullet}(x,t)][M(x,t)] - k_{tp}[R^{\bullet}(x,t)][M^{\bullet}(x,t)] - k_t[M^{\bullet}(x,t)]^2 \tag{10}$$

where k_t (cm^3/mol s) is the rate constant of bimolecular termination. For the sake of simplicity, chain transfer to monomers is neglected in eq 10, i.e., $k_{tr} = 0$, since large initiator concentration is produced, regeneration of $R^{\bullet}$ is assumed to be negligible. It is necessary to point out that the polymerization rate, $R_p = k_p[M^{\bullet}(x,t)][M(x,t)]$, does not appear in eq 10. This is because the propagation reaction consumes a macro-radical to yield another growing active tip, i.e., another macro-radical. The consumption is therefore balanced by the generation and so a removal term in eq 10 is not necessary.

Once again, the two chemical reactions experienced by the monomer molecules are: (a) their reaction with primary radicals; and (b) their polymerization and thus involvement in propagation through their reaction with macro-radicals. When the material layer is exposed by the interfering irradiance, the monomers in the bright regions are polymerized by the generated primary radicals. This induces monomer concentration gradients, and as a result the monomers in the dark regions diffuse into the monomer-depleted exposed regions. This diffusion behavior can be modeled using Fick's second law which is included in the 1-D NPDD model.[7−9,16,17] The rate equation governing the monomer concentration is shown,

$$\frac{d[M(x,t)]}{dt} = \frac{d}{dx}\left\{D_m(x,t)\frac{d[M(x,t)]}{dx}\right\} - k_i[R^{\bullet}(x,t)][M(x,t)] - \int_{-\infty}^{\infty} G(x,x')k_p[M^{\bullet}(x,t)][M(x,t)]\,dx' \tag{11}$$

where $D_m(x,t)$ (cm^2/s) represents the monomer diffusion, $G(x,x')$ is the nonlocal material spatial response function,[19]

$$G(x,x') = \frac{1}{\sqrt{2\pi\sigma}}\exp\left[\frac{-(x-x')^2}{2\sigma}\right] \tag{12}$$

which represents the spatial effect of the initiation at location x' on the amount of monomers polymerized at location x, and σ is the nonlocal response parameter.[7−9,16,17,20] Also, x, x', and $\sigma^{1/2}$ representing the lengths, which are normalized with respect to the grating period, Λ.

2.3. Inhibition. During the holographic exposure, an inhibition period, i.e., a dead-band, is observed at the beginning of the grating growth curve. This process acts to inhibit the production of polymer chains until sufficient concentration of inhibitor, $[Z]$, is removed to allow the unhindered polymerization to take place. The reactions causing inhibition arise mainly due to the suppression of the production of macro-radicals and polymer chains by the *scavenging effects*, when $R^{\bullet}$ and $M^{\bullet}$ are scavenged by Z, at a relatively high rate constant k_z,

$$R^{\bullet}\ (\text{or } M_n^{\bullet}) + Z \xrightarrow{k_z} R\ (\text{or } M_n) + Z^{\bullet}, \quad \text{and/or } R{-}Z^{\bullet}\ (\text{or } M_n{-}Z^{\bullet}) \tag{13}$$

where $Z^{\bullet}$, $R{-}Z^{\bullet}$, and $M_n{-}Z^{\bullet}$ are assumed not to cause any reinitiation and/or lead to any regeneration; i.e., no further chain transfer mechanisms involve them with other molecules. All the inhibitors are rapidly consumed during the initial stage of the exposure. We recall that inhibition is assumed to arise due to the initially dissolved molecular oxygen present in the photopolymer layer.[5−10] Under holographic exposure, when Z is consumed by ^{3}Dye*, $R^{\bullet}$, and $M^{\bullet}$, [see eqs 1.5 and 13], temporal and spatial variations of the inhibitor concentration will be formed. Diffusion of the molecular oxygen from dark regions into bright regions then

takes place. Since the oxygen molecules are small, they are relatively free to diffuse rapidly through the material layer matrix. This results in the following rate equation of inhibitor concentration,

$$\frac{d[Z(x,t)]}{dt} = \frac{d}{dx}\left\{D_z(x,t)\frac{d[Z(x,t)]}{dx}\right\} - k_z[^3Dye^*(x,t)][Z(x,t)] - k_z[R^\bullet(x,t)][Z(x,t)] - k_z[M^\bullet(x,t)][Z(x,t)] + \tau_z\{[Z_0] - [Z(x,t)]\} \quad (14)$$

where $D_z(x,t)$ (cm^2/s) is the diffusion constant of inhibiting oxygen in the dry material layer; and the additive term, i.e., τ_z [[Z_0] − [$Z(x,t)$]], represents the replenishing of inhibiting oxygen from the outside the layer, i.e., from the air into the material when the layer is uncover plated (unsealed).[9,10] τ_z (s^{-1}) represents the rate at which the oxygen is replenished. It is assumed that the oxygen concentration in the layer can never be greater than the initially dissolved oxygen concentration, [Z_0] (mol/cm^3).[9,10] The inhibition rate constants for each inhibition process will in general have different values due to different reactivities. However, in this analysis for the sake of simplicity, they are all treated as being equal to k_z.

2.4. Termination. Polymer chains will continue to grow until the supply of accessible monomers is exhausted. Three possible termination mechanisms are present:

(i) When two growing macro-radicals meet and interact with each other, they can terminate either by: (a) combination at a rate constant of k_{tc}, i.e., addition of two macro-radicals becomes one lumped terminated polymer chain, or terminate by (b) disproportionation at a rate constant of k_{td}, i.e., following collision of two macro-radicals becoming two separate terminated polymer chains. These two mechanisms are both referred to as bimolecular termination.[7,13−17] In this study, since the specific mode of termination and *effects of chain transfer to polymers* do not affect the photopolymerization kinetics, for the sake of simplicity, we treat the two mechanisms as one by combining the two rate constants,

$$M_n^\bullet + M_m^\bullet \xrightarrow{k_t} M_n + M_m \text{ (or } M_{n+m}) \quad (15)$$

where $k_t = k_{tc} + k_{td}$. We note that this combination of termination, and/or chain transfer to polymers may lead to a little shortening on the chain length formed.[14] However as mentioned earlier, in our analysis no distinction is made between different chain lengths, since it does not affect the predictions of the resulting model.

(ii) When a growing macro-radical reacts with a primary radical, an inactive or terminated polymer chain is then formed.

$$R^\bullet + M_n^\bullet \xrightarrow{k_{tp}} M_nR \quad (16)$$

The regeneration and/or recombination of primary radicals, $R^\bullet$, by chain transfer to polymers and/or initiators is also neglected in this analysis, i.e., $R^\bullet$ is only involved in inhibition, initiation and termination, as it has been shown that it is negligible compared to other photopolymerization kinetics taking place.[7−9,12,17] Furthermore, the rate constant of primary termination k_{tp} (mol/cm^3 s) is generally greater than k_t for bimolecular termination since: (a) The interaction of $R^\bullet$ with $M_n^\bullet$ can be very different from that of $M_n^\bullet$ with $M_m^\bullet$, due to different reactivity; and (b) $R^\bullet$ is much smaller and more mobile compared to $M_n^\bullet$, and therefore the diffusion controlled effects (due to viscosity changes) will impact them quite differently.

In the previous studies,[7−9,16,17] it was shown that when the photopolymer layer is exposed with moderate (or even low) intensities, the linear dependence of the polymerization rate, R_p, on the monomer concentration and its square root dependence on the initiation rate, R_i, agree quite well with the experimentally estimated parameter values. In this case, the generated concentration of initiator, primary radicals, $R^\bullet$, will be relatively low. As a result, the macro-radicals are much more likely to undergo a reaction involving macro-radicals in chain to chain, bimolecular termination, rather than primary termination, i.e., termination with the primary radicals in a chain to radical reaction. Under these conditions, the steady state assumption described by eq 9 remains valid.

However, the square root dependence of polymerization, R_p, on initiation, R_i, breaks down,[7,19] when a high concentration of initiator is rapidly produced. In this case, the steady state assumption which describes the ideal photopolymerization kinetics behavior is violated. When the photopolymer layer is exposed with high intensity, a significantly large concentration of primary radicals is produced, which not only increases the initiation rate, but also greatly increases the likelihood of primary termination[7,12,19,21] taking place. This rapidly produced high concentration of primary radicals can therefore act to limit the propagation of macro-radicals, resulting in the shortening of polymer chains formed (i.e., a reduction in the average molecular weight). This has several consequences: (1) reducing the polymerization rate results in a reduction in the overall concentration of polymer produced, and (2) shortened polymer chains are more mobile than the longer chains produced. That is to say that the grating index modulation may decrease due to polymer diffusion, in the absence of sufficient cross-linking.[16] Furthermore, these rapidly produced primary radicals also result in the rapid conversion of monomers to polymers, i.e., R_p increases, which simultaneously causes a more rapid increase in viscosity,[7−9,12] compared to that which takes place under the weaker exposing intensity conditions. Finally, the rate equation governing the kinetics of polymer concentration can be written as,

$$\frac{d[P(x,t)]}{dt} = \int_{-\infty}^{\infty} G(x,x')k_p[M^\bullet(x,t)][M(x,t)]\,dx' \quad (17)$$

where [$P(x,t)$] (or [$N(x,t)$][7−9]) is the polymer concentration. As noted, if the polymer chains are not cross-linked sufficiently, they will tend to diffuse out of the exposed regions in order to reduce the polymer gradient.[17] If this takes place, it will result in a decay of the grating refractive index modulation, with time. Such an effect becomes more expeditious at high recording spatial frequencies.[17] In the analysis presented here, we assume that the diffusion of polymer chains does not take place, since based on the experimental observations, the polymer chains are highly cross-linked, and the recorded gratings are stable with no observed decay of refractive index modulation postexposure.

The rate equations governing the chemical species concentrations and their associated with photochemical reactions, have now been presented, i.e., eqs 2−7, 10, 11, 14, and 17. Given a cosinusoidal illumination, the concentrations will all be periodic even functions of x and can therefore be written as Fourier series,

$$[X(x,t)] = \sum_{i=0}^{\infty} X_i(t)\cos(iKx) \quad (18)$$

where X represents the species concentrations: [Dye, ^{1}Dye*, ^{3}Dye*, HDye$^\bullet$, ED, $R^\bullet$, $M^\bullet$, M, Z, and P]; and i indicates the harmonics in the Fourier series expansions. A set of first

order coupled differential equations can be derived by incorporating the photoinitiation model[5,6] into the 1-D NPDD model, gathering the coefficients of the various cosinusoidal spatial contributions and then writing the equations in terms of these time varying spatial harmonic amplitudes. In order to solve this set of first order coupled differential equations, appropriate initial conditions (i.e., before exposure) are required: [Dye](t = 0) = [A_0], [^{1}Dye*](t = 0) = 0, [^{3}Dye*](t = 0) = 0, [HDye$^\bullet$](t = 0) = 0, [ED](t = 0) = [ED_0], [R$^\bullet$](t = 0) = 0, [M$^\bullet$](t = 0) = 0, [M](t = 0) = [U_0], and [P](t = 0) = 0, where [A_0], [ED_0], and [U_0] are the initial concentrations of photosensitizer, electron donor, and monomer, respectively. As in previous analyses,[7−9,16,17,20] calculations of the monomer and polymer harmonic amplitudes involves use of the nonlocal spatial response function, $G(x,x')$ in eq 12, the effects which appear in the coupled differential equations in the form of the parameter, $S_i = \exp(-i^2K^2\sigma/2)$.

3. Model Simulations

In this section, the predictions of the model presented in the previous section are numerically examined, in order to explore the kinetics behavior caused by varying the material parameter values. In this way, their effects on grating index modulations can be obtained, and insights made regarding the grating formation achieved.

Before presenting the simulation results, we note that in all the calculations presented, the time varying viscosity effects are assumed negligible, therefore the diffusion coefficients do not vary as functions of either time or space, i.e., $D_m(x,t) = D_{m0}$, $D_z(x,t) = D_{z0}$, where D_{m0} and D_{z0} are the diffusion constants for monomer and inhibitor, respectively. It is assumed that an unslanted transmission type volume holographic grating is recorded. The spatial frequency chosen for the simulations is 1428 lines/mm (corresponding to a period of Λ = 700 nm). This value is chosen in order to correspond to the experimental results discussed in the following section. The exposing fringe visibility is, V = 1. The nonlocal parameter is chosen to be S_1 = 0.94, which was previously determined.[7−9,16,17] This value is equivalent to a nonlocal response length of $(\sigma')^{1/2}$ = 54 nm (where $\sigma = \sigma'/\Lambda^2$).[7−9,16,17] The number of spatial concentration harmonics retained, in the Fourier series expansions, eq 18, is 12 (i.e., $0 \le i \le 11$). This value is chosen based on the comparisons of results from simulations using 4, 8, and 12 harmonics,[7] which show that the system is numerically stable and the model converges rapidly with the inclusion of higher-order harmonics. Several other physical parameter values are appropriately assigned based on the results of previous studies.[5−10,17] The initial concentrations of the photosensitizer (erythrosine B, $C_{20}H_6I_4Na_2O_5$), [A_0] = 1.22×10^{-6} mol/cm^3; monomer, [U_0] = 2.83×10^{-3} mol/cm^3; electron donor, [ED_0] = 3.18×10^{-3} mol/cm^3 and inhibitor: [Z_0] = 1×10^{-8} mol/cm^3.

Typical rate constants are chosen for the simulations: k_{st} = 5.35×10^6 (cm^3/mol s), $r_1 = 1.2 \times 10^{-3}$ (s^{-1}), r_2 = 8.3×10^{-4} (s^{-1}), $k_b = 1.66 \times 10^4$ (cm^3/mol s), $k_d = 8.6 \times 10^3$ (cm^3/mol s), $k_i = 1.56 \times 10^7$ cm^3/mol s, $k_p = 2.26 \times 10^7$ (cm^3/mol s), $k_z = 6.98 \times 10^8$ (cm^3/mol s), $k_t = 8.02 \times 10^7$ (cm^3/mol s), and $k_{tp} = 2.05 \times 10^{10}$ (cm^3/mol s). The diffusion coefficients for monomer and inhibitor are, $D_{m0} = 8.3 \times 10^{-11}$ (cm^2/s), $D_{z0} = 1.0 \times 10^{-8}$ (cm^2/s) respectively. We note that the influence of chain transfer on these kinetic parameters is neglected, thus their values do not vary during polymerization. The experimental conditions include that: the dry material layer for thickness, d = 100 μm, is exposed by recording beams of wavelength, λ = 532 nm and probed with a wavelength of, λ = 633 nm. Previously determined absorption parameters[10] for erythrosine B are also used: $\varepsilon = 1.4 \times 10^8$ cm^2/mol, ϕ = 0.036 mol/einstein, and T_{sf} = 0.76.

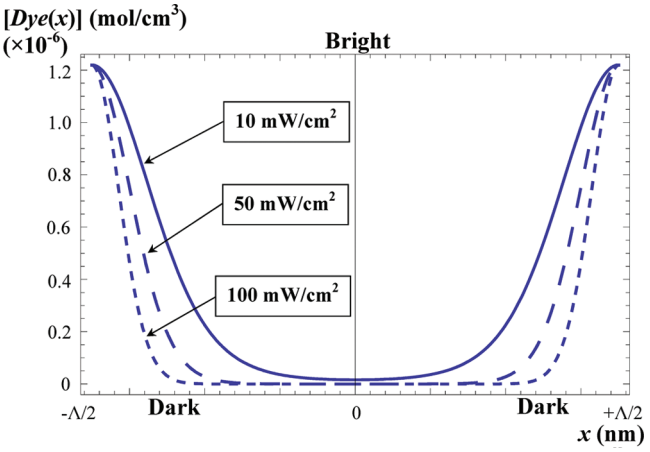

Figure 1. Spatial variation of the ground state dye concentration for exposure intensities of 10 (solid line), 50 (dashed line), and 100 mW/cm^2 (short dashed line), at the grating period Λ = 700 nm.

Using these parameter values, the spatial distribution of ground state dye, [Dye(x)], is found after substituting eq 18 into eq 2, and subsequently adding the amplitudes of all the harmonics. [Dye(x)] is plotted between $\pm$ Λ/2 in Figure 1. The results for three relatively high exposing intensities: I_{01} = 10 mW/cm^2, I_{02} = 50 mW/cm^2, and I_{03} = 100 mW/cm^2 are shown. In order to provide a meaningful comparison, the exposure time, t, for each case is adjusted to ensure equal dosage being delivered, where the dosage, $\xi = I_0^{1/2}t$.[16]

As can be observed from Figure 1, the high intensity exposures lead to a rapid consumption of the ground state dye concentration in the bright regions, and the spatial variation of the ground state dye concentration distorts from the exposing sinusoidal pattern purity exhibiting narrowing in the dark regions. Furthermore, as the exposure intensity increases, the distortion is visibly stronger, leading to even more ground state dye concentration being consumed in the dark bands. Clearly there is a nonlinear response of the material to the exposure intensity. Consequently, the spatial distribution of the primary radical concentration generated leads to deviations in the polymer concentration from the ideal sinusoidal distribution, which would be produced given a linear material response. Therefore, the polymer chain initiation is not directly proportional to the exposing interference patterns. Hence, the loss in the sinusoidal fidelity of the grating profile that will be eventually formed.

Retaining the same parameter values and simulation conditions described above, the evolution of the polymerization rate, $R_p = k_p$[M$^\bullet$][M], can be examined (see Figure 2) using the model by numerically solving for [M$^\bullet$] and [M] respectively, i.e., summing the concentration amplitudes of all their harmonics (i = 0 to i = 11).

As can be seen from Figure 2, when the recording intensity increases from I_{01} to I_{03}, the polymerization rate increases more rapidly toward a higher maximum value and then decreases more rapidly. This is due to the more rapid initiation process taking place in the same time frame (t = 0 to t = 20 s in Figure 2). For higher exposure intensity, a larger quantity of the photons available are absorbed, hence a greater number of radicals and macro-radicals are then produced. However, as mentioned previously, this also increases the likelihood of termination processes, in particular primary termination. Therefore, a larger value of R_p generally causes a more rapid conversion from monomers to polymers. However throughout the conversion, R_p will then decrease much more quickly after reaching its larger maximum value. This is mostly due to the more rapid consumption of absorptive dye, radicalization of monomers and

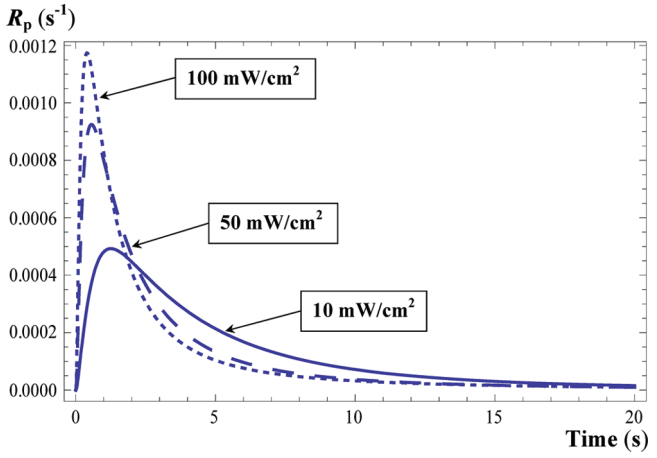

Figure 2. Comparisons of polymerization rate for intensities of 10 (solid line), 50 (dashed line), and 100 mW/cm^2 (short dashed line).

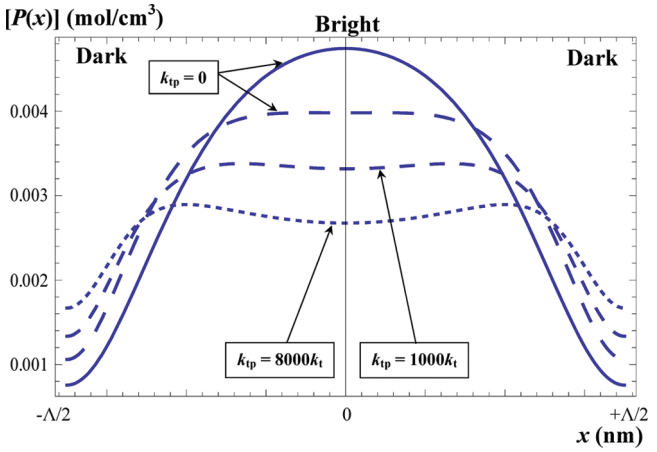

Figure 3. Spatial variation of the polymer concentration for various values of $k_{tp} = 0$ (solid line), $k_{tp} = 1000k_t$ (dashed line) and $k_{tp} = 8000k_t$ (short dashed line), at the grating period $\Lambda = 700$ nm.

termination of the active growing macro-radicals, which all result from the high exposure intensity.

The corresponding spatial distributions of polymer concentration can also be predicted, and are presented in Figure 3. In order to demonstrate the effects of primary termination, comparisons are made for three substantially different rate constants of primary termination, k_{tp}. The intensities chosen for this simulation are 10 and 100 mW/cm^2. As can be observed from Figure 3:

(**I**) When the exposing intensity increases from 10 (solid curve) to 100 mW/cm^2 (dashed curves), due to the increasingly nonlinear effects, the spatial distribution of the polymer concentration is not sinusoidal but significantly distorted from ideal sinusoidal behavior. Some insight into these effects can be achieved using the parameter, $\mathbb{R} = (D_m K^2)/(\kappa I_0)$, which was originally introduced by Zhao et al. in ref 22. κ is assumed to be a material constant. $\mathbb{R}$ is used to quantify the relationship between monomer diffusion and polymerization (nonsteady state, where $R_p \propto I_0$). For the sake of simplicity, it can be considered that as, $\mathbb{R} \propto (4\pi^2 D_m)/(\Lambda^2 I_0)$, which can be used to characterize the material responses to the exposure intensity.[22,23] In this analysis, the value of $\mathbb{R}$ is relatively small (due to the large value of I_0). This indicates that during the grating formation, in the bright regions the rate at which the monomers being polymerized becomes significant compare to the rate at which the monomers diffuse in from the dark regions. As a result, a distorted polymer concentration distribution is formed. In this situation, any monomers diffusing into the bright regions are rapidly polymerized (by the large quantity of available primary radicals), before they can diffuse further into the central area of the exposing patterns. Therefore, a dip appears in the center and peaks rise on the both sides of the spatial polymer concentration distribution.

Since $\mathbb{R}$ is inversely proportional to I_0,[20,22,23] increasing I_0 results in the values of all concentration harmonics of polymer decreasing, but the amplitudes of the higher order harmonics become relatively stronger, ultimately resulting in a reduction in the saturation value of refractive index modulation achieved. This can be explained by noting that, the high exposing intensity not only causes a more rapid consumption of monomers, resulting in stronger concentration gradients, and giving rise to monomer diffusion, but also increases the likelihood of dye consumption close to the dark regions, where the monomers will be radicalized. We recall that, the narrowing of the dye concentration peaks in the dark regions also causes the spatial distribution of primary radicals generated, to deviate from the ideal sinusoidal profile.

(**II**) The effects of the inclusion of primary termination for the same exposure intensity (100 mW/cm^2) are presented in the figure by comparing results for three cases: (1) no primary termination taking place, i.e., $k_{tp} = 0$, (long dashed curve), (2) inclusion of primary termination with $k_{tp} = 1000\ k_t$ (dashed), and (3) $k_{tp} = 8000\ k_t$ (short dashed). It is clear that the inclusion of primary termination leads to a reduction in the amplitudes of the polymer concentration distribution, and the larger the value of k_{tp}, the greater the reduction predicted. From this trend, it is plausible to say that with a faster primary termination rate (which is usually faster than the initiation rate), more macro-radicals are likely to be terminated by primary radicals before they can propagate very far. Moreover, the monomers which diffuse in from dark regions during the conversion also experience the rapid primary termination process. This effect is particularly strong in case 3, which suggests that more macro-radicals are terminated close to the edges of the bright regions, consequently resulting in an uneven spatial concentration distribution (from the edges to the center). Thus, the dip in the center of the polymer concentration profile broadens. On the basis of this analysis, it is reasonable to predict some of the potential possibilities when primary termination is highly effective:[11−13,19,21,24] in the bright regions, (a) a lower concentration of polymer is produced, since fewer primary radicals are in fact used for initiation, and (b) the average polymer chain length is also reduced, due to the growing active macro-radicals being rapidly terminated before they can propagate significantly. Furthermore, the increase of the polymer concentration in the dark regions can be explained as: it is also caused by the nonsinusoidal primary radical distribution, which results in more monomers being polymerized there. This nonsinusoidal behavior is also visibly stronger as the value of k_{tp} increases, and the contrast in polymer concentrations between bright and dark regions decreases.

In order to further examine the effects of primary termination for the high exposure intensities, the analysis is now carried out in an alternative way. A uniform illumination is applied to a material layer with no spatial variations, i.e., $V = 0$. In this way, the exposed region is eventually homogeneously polymerized. Therefore, in the theoretical model, only the contributions from the zeroth order harmonic of the rate equation for each chemical species are considered. The simulations are performed by individually calculating the accumulative concentration caused by primary termination for each particular high intensity applied, i.e., integrate the term $k_{tp}[R^\bullet][M^\bullet]$, over the exposure time, t. In this way, the macro-radical concentration terminated by primary radicals, [PT] (mol/cm^3), for each high exposure intensity examined, can be estimated. Four cases are chosen for examinations: (a) $k_{tp} = k_t = 8.02 \times 10^7$ cm^3/mol s, (b) $k_{tp} = 10\ k_t$, (c) $k_{tp} = 100\ k_t$ and (d) $k_{tp} = 1000k_t$.

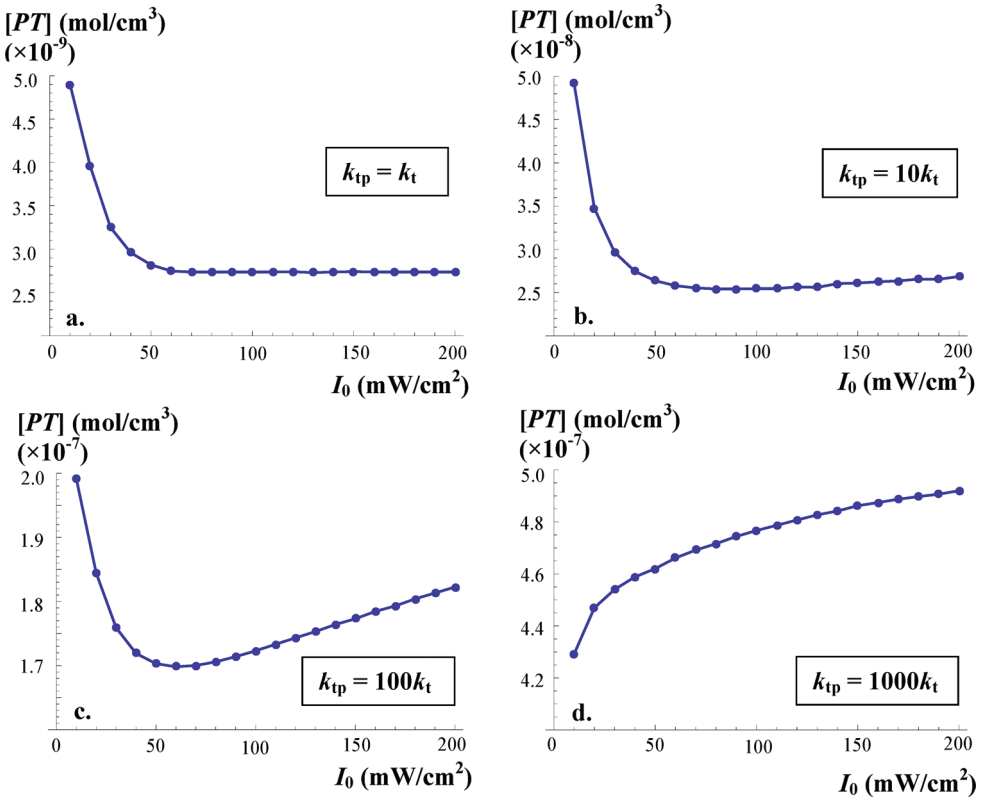

Figure 4. Intensity response of primary termination for cases (a) $k_{tp} = k_t$, (b) $k_{tp} = 10k_t$, (c) $k_{tp} = 100k_t$, and (d) $k_{tp} = 1000k_t$.

The results for intensities from 10 up to 200 mW/cm^2 are examined. The exposure time is also suitably adjusted to ensure equal dosage, $\xi = I_0^{1/2}t$,[16] being delivered to the material. The results are presented in Figure 4. As can be observed in going from cases a−d, the overall macro-radical concentration terminated by primary radicals, [PT], generally increases, for the increased values of k_{tp}.

In cases a and b, when the primary termination rate is comparable to the bimolecular termination rate, i.e., $k_{tp} = k_t$ and $k_{tp} = 10k_t$, the behavior predicted is quite similar: the concentrations of macro-radicals terminated by primary termination decreases for the I_0 values from 10 to 60 mW/cm^2. As can be observed further increases in exposing intensity above 60 mW/cm^2 do not cause any further reduction. Examining Figures (4a) and (4b), it can be seen that [PT] tends to decrease as the exposing intensity increases. This is as a result of more primary radicals being used for initiation rather than for termination. For intensities higher than 60 mW/cm^2, [PT] remains almost constant. This is because the available concentration of growing macro-radicals which could be terminated by primary radicals has become exhausted, since most of the macro-radicals have already undergone the propagation or bimolecular termination processes.

However, in case c, when $k_{tp} = 100k_t$, primary termination starts performing differently from cases a and b, once the exposure intensity is greater than 60 mW/cm^2. As can be seen, the amount of [PT] increases as the exposing intensity increases. This behavior indicates that when k_{tp} is significantly greater than k_t and the exposing intensity is high enough, more growing macro-radicals will be involved in primary termination (see Figure (4c), before they continue propagating any longer or terminate one another by bimolecular termination. As demonstrated in case d, the high intensity response of primary termination becomes even more significant than in case c, when $k_{tp} = 1000k_t$, [PT] increases almost linearly as the exposure intensity increases, as shown in Figure (4d). In this regime, primary radicals are much more available for termination, and are not limited by the available macro-radical concentration as in the scenarios predicted for cases a and b.

On the basis of the observations and analyses presented above, a sensible and reasonable indication can be obtained, which assists in determining the termination kinetic parameters. It shows the necessity of including primary termination when modeling the nonsteady state conditions, especially when high exposing intensities are applied. Ultimately, in order to estimate k_{tp}, the values are extracted by best fitting to the experimental growth curves of refractive index modulation using the predictions of the model and searching over sensible parameter search ranges. This process is described in detail in the following section.

4. Experimental Work

In this section, a least-squares fitting algorithm is applied, involving the use of a mean square error (MSE) cost function to quantify the difference between the theoretical predictions of our model and the experimentally obtained data. The MSE is iteratively minimized, and from the best fits achieved, acceptable parameter values are determined, by searching over physical search ranges. A typical experimental setup for recording unslanted transmission holographic gratings is exactly carried out as previous, which was schematically presented in ref 25. The material used in all the experiments is a standard PVA/AA photopolymer,[5−10,16,17,25] with photosensitizer, erythrosine B.

4.1. Absorption and Transmission. When recording an unslanted holographic grating in a photopolymer material, the intensities of the two exposing beams produces an approximately sinusoidal interference pattern.[26] These two modulated recording beams result the spatial distribution of ground state dye concentration following photon absorption in the material layer. In order to examine the photoabsorption behavior for equivalent uniform (single beam) and holographic (double beams) exposures, experimental data for normalized transmission curves are fit (see Figure 5) using the incorporated photoinitiation model [eqs 2−5] taking account of dye recovery and

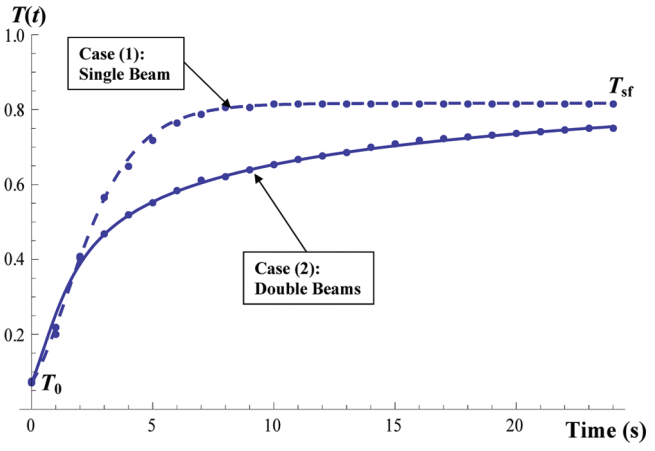

Figure 5. Fits to the experimental data (dots) of normalized transmission curves of case (1), single beam exposure, and case (2), two beams holographic exposure.

photobleaching effects with previously determined rate constants.[5,6]

Figure 5 illustrates the two sets of experimental transmission curve data: case 1, single (uniform) exposing beam ($V = 0$) at the incident angle, $\theta = 22.33°$ (in the layer with respect to normal incidence for wavelength $\lambda = 532$ nm); and case 2, double (holographic) recording beams ($V = 1$) at the same incident angles, $\pm\theta$, giving a spatial frequency of 1428 lines/mm. The total exposing intensity in each case is adjusted to be 60 mW/cm^2. Applying the Lambert−Beer law, the normalized transmission can be expressed using,[6]

$$T(t) = T_{sf} \exp\{-\varepsilon[\mathrm{Dye}(t)]d'\} \tag{19}$$

Eq 19 is used to fit the experimental data, where T_{sf} is experimentally observed to be 0.8. [Dye(t)] can be numerically found using eq 2 and the optical path length is revised to be, $d' = d/\cos\theta$, to allow for the incident angle, θ. As can be seen in both cases, transmission $T(t)$ starts at T_0, due to the same homogeneous initial photosensitizer concentration, [A$_0$]. However, as the exposure time increases, the two transmission curves start to differ from one another. In case 1, the consumption of the ground state dye concentration is uniformly distributed across the exposure region, therefore, the transmission rapidly grows and reaches the saturation value T_{sf} much sooner. Applying the fit to the experimental data by assuming that $V = 0$ (single beam incidence), the rate of production of excited state photosensitizer is then estimated to be $k_a = 8.06 \times 10^2$ s^{-1}. In case 2, the growth of transmission involves the nonlinear spatial distribution of ground state dye during absorption. Therefore, in case 2, when the layer is holographically exposed, the spatial modulation of the recording beams causes a nonuniform absorption across the exposed region, i.e., in the dark regions, most of the dye molecules do not get excited. As a result of this, k_a, is reduced and is determined to be, $k_a = 6.28 \times 10^2$ s^{-1}. From the trend of the curve indicates that, the transmission in case 2 will eventually reach the same T_{sf} if the exposure time is long enough; i.e., T_{sf} is a constant value for a particular material composition.[8,27,28] In this situation, the spatial distribution of dye concentration in the dark bands will become "infinitesimally narrow" (see Figure 1), where most of the dye concentration has been consumed. In addition, the diffusion of dye molecules (due to the concentration gradient) from the dark regions into the bright regions will eventually take place over an appreciably long time.[29]

4.2. Refractive Index Modulation. During holographic exposure, the growth of the grating is monitored experimentally at the Bragg condition (i.e., on-Bragg replay) by a probe beam at a wavelength to which the photosensitizer used in the layer is insensitive. The temporal evolutions of the resulting first order diffracted intensity, I_d, and the transmitted intensity, I_t, of the probe beam are simultaneously measured. Thus, the diffraction efficiency can be calculated using $\eta(t) = I_d(t)/I_{0P}$, where I_{0p} is the incident intensity of the probe beam. The time varying diffraction efficiency, $\eta(t)$, can be described in relation to the first-order harmonic of grating refractive index modulation, $n_1(t)$, using the first order coupled wave theory,[30]

$$\eta(t) = \sin^2\left[\frac{\pi d n_1(t)}{\lambda_p \cos\theta_{in}}\right] \tag{20}$$

where d is the thickness of the material layer, λ_p is the wavelength of the probe/replay beam and θ_{in} is the corresponding on-Bragg replay angle inside the layer. All the swelling and shrinkage effects occurring during recording, i.e., due to the creation and collapse of holes,[7,31] are neglected. We assume the total volume fraction is conserved,

$$\varphi_m(t) + \varphi_p(t) + \varphi_b(t) = 1 \tag{21}$$

where φ_m, φ_p and φ_b are the volume fractions of the monomer, polymer and the background material in the layer, respectively. The volume fractions is given by, $\varphi_i = x_i v_i / \Sigma_i x_i v_i$, where x_i is the mole fraction and v_i is the molar volume fraction of the i^{th} component. Applying the Lorentz−Lorenz relation, the temporal evolution of the first-order harmonic of grating refractive index modulation can be expressed as,[7,9,17,31]

$$n_1(t) = \frac{({n_{dark}}^2+2)^2}{6n_{dark}}\left[\varphi_{m1}(t)\left(\frac{{n_m}^2-1}{{n_m}^2+2}-\frac{{n_b}^2-1}{{n_b}^2+2}\right) + \varphi_{p1}(t)\left(\frac{{n_p}^2-1}{{n_p}^2+2}-\frac{{n_b}^2-1}{{n_b}^2+2}\right)\right] \tag{22}$$

where n_{dark} is the refractive index of material layer before exposure;[31] n_m, n_p and n_b are the refractive indices for the monomer, polymer and the layer background material[31] respectively. We note that $n_p > n_m$, because during the conversion from monomer to polymer, the breaking of the C=C bonds in the monomer molecules produces a change in the density, hence the refractive index of the photopolymer layer. No differentiation is made between the contributions to the refractive index changes made by polymer chains of different molecular weight/lengths. $\varphi_{m1}(t)$ and $\varphi_{p1}(t)$ are the time varying first harmonic volume fractions of monomer and polymer, which can be found by relating the first harmonic of monomer and polymer concentrations calculated using eqs 11 and 17. Initial conditions are also needed: $\varphi_{m1}(0) = \varphi_{m0} = 0.273$, $\varphi_{p1}(0) = 0$, and $\varphi_b = 0.727$ (which is constant through all the processes), where φ_{m0} is the monomer volume fraction before exposure which can be directly estimated, based on the initial material composition.[8,9,17,25]

A set of growth curves of refractive index modulation are obtained from the same experimental conditions described in section 3. A range of high exposing intensities are examined, i.e., from 10 mW/cm^2 up to 150 mW/cm^2. For clarity and brevity, four typical cases are present. Figure 6 contains the fits to the average experimental index modulation growth curves obtained (from reproducible experimental results) for each of the following exposing intensities: $I_{01} = 10$ mW/cm^2, $I_{02} = 50$ mW/cm^2, $I_{03} = 100$ mW/cm^2, and $I_{04} = 150$ mW/cm^2.

As can be observed from Figure 6:

(1) At the start of the growth of refractive index modulation, there is a noticeable dead band, t_i, caused by the inhibition processes due to the inhibitor, Z. With the increase of the exposing intensities, t_i reduces due to the more rapid consumption of Z. This behavior is clearly more significantly observable for low exposing intensities.[9,16] Since high exposing intensities are studied in this work, the replenishing

of inhibiting oxygen from the air into the photopolymer layer, does not significantly affect the change of t_i as strongly. Since as soon as the oxygen diffuses into the layer, the rapidly produced excited states dye molecules and primary radicals will react with them. Thus, they are unlikely to replenish the inhibitor concentration,[9] and thus τ_z $\{[Z_0] - [Z(x,t)]\}$ in eq 14 can be neglected in this case.

(2) It is noticeable that, as the exposing intensity increases from $I_{01} = 10$ mW/cm^2 to $I_{04} = 150$ mW/cm^2, the rate of the growth of refractive index modulation becomes more rapid, and reaches the saturation, n_{1sat}, sooner. This trend is mainly ascribed to the highly increased polymerization rate, R_p (shown in Figure 2), where monomers are rapidly converted into polymers to form the grating. It is also noted from the experimental results, that further increases of the exposing intensity above 150 mW/cm^2 does not give rise to even faster growth of refractive index modulation. It suggests that the photosensitive dye has reached its absorption limit (due to the constant absorptivity, ε), i.e., the maximum amount of photons the dye molecules can absorb, at a fixed initial dye concentration, $[A_0]$.

(3) Once again, it is worth emphasizing that, these high exposing intensities, not only increase the initiation, but also increase the likelihood of primary termination. This results in the average polymer chain length being shortened, and the polymer concentration that can be produced also being reduced. Thus, as a consequence of greatly increasing the exposing intensity, the saturation value of refractive index modulation achieved, ultimately also decreases, i.e., n_{1sat} drops. This can be clearly seen from the cases of $I_{02} = 50$ mW/cm^2 to $I_{03} = 100$ mW/cm^2, where in this intensity region, primary termination has become more significant during the polymerization processes.

On the basis of the fits [using eq 22] to the experimental data, the important kinetic parameter values are extracted. The results are presented in Table 1, along with the corresponding MSE values provided to indicate the quality of the fits to the experimental data.

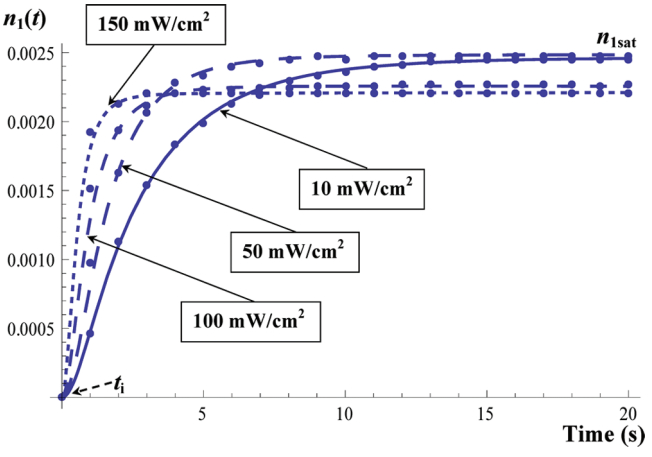

Figure 6. Fit to experimentally obtained growth curves (dots) of refractive index modulation for four different exposing intensities: 10 (solid curve), 50 (long dashed curve), 100 (dashed curve), and 150 mW/cm^2 (short dashed curve).

Moreover, to utilize the predictions of [PT] presented in Figure 4, in combination with the knowledge of these parameters presented in the literature,[7−9,11−20,24,25] the search ranges for extracting each parameter value were carefully and sensibly applied. Particularly during the estimations of k_t and k_{tp}, while aiming to achieve quality fits for each case in Figure 6, the relationships between these two parameters illustrated in Figure 4 are also substantiated, respectively. As can be noted in Table 1, the results determined for k_t and k_{tp} concur with the scenario demonstrated by Figure (4d), where $k_{tp} \approx 1000k_t$, which is therefore identified as being the most physically valid scenario. This echoes the previous theoretical analyses, for greatly enhanced primary termination mechanism.

In order to provide an overview of the material response for the high intensities examined, Figure 7 presents a combination of theoretical predictions and experimental results for the saturation values of refractive index modulation achieved, n_{1sat}, corresponding to each exposure intensity, I_0, examined. As can be observed from this response in Figure 7, the agreement achieved between the theoretical predictions and experimental results is quite satisfactory. The value n_{1sat} starts to appreciably drop as the exposing intensity increases. This clearly shows the progressively amplified primary termination effects, since which is believed to be the main attributor in this study.

4.3. Polymer Diffusion. To further verify our explanations of the consequences caused by primary termination, additional experiments were also performed. The standard PVA/AA material was modified, such that the cross-linker (Bis(acrylamide), $C_7H_{10}N_2O_2$) was not included,[17] and an extra amount of monomer (Acrylamide, C_3H_5NO) was added to compensate for the resulting loss in volume fraction. Since uncross-linked polymer chains are much more mobile and flexible, thus they tend to diffuse out of the bright regions where they are formed. The resulting decay of refractive index modulation was then monitored over an appreciable postexposure time. The decay of the grating index can be described using a simple model,[17]

$$n_1(t) = n_1(t \rightarrow \infty) + \Delta n_1 \exp(-\alpha_P t) \qquad (23)$$

where $n_1(t\rightarrow\infty)$ is the minimum value that the refractive index modulation decays to over the long time frame examined, and

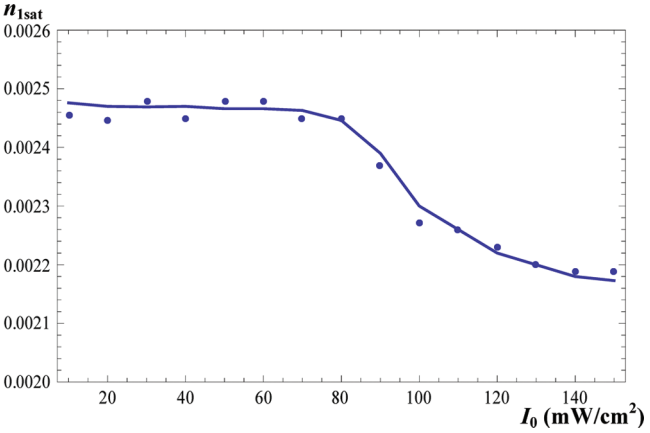

Figure 7. Combination of experimental results (dots) with theoretical prediction (solid curve) for the high intensity (I_0) response of the achieved saturation values of refractive index modulation (n_{1sat}).

Table 1. Extracted Parameter Values from Fits to Experimental Refractive Index Modulation Growth Curves

I_0 (mW/cm^2)	k_i (cm^3/mol s) × 10^7	k_p (cm^3/mol s) × 10^7	k_t (cm^3/mol s) × 10^7	k_{tp} (cm^3/mol s) × 10^{10}	D_m (cm^2/s) × 10^{-11}	MSE (-) × 10^{-10}
10	4.86	1.57	9.09	7.05	8.93	7.17
50	4.95	1.98	6.84	8.06	7.51	3.54
100	4.66	1.70	6.36	8.65	6.27	5.18
150	4.98	1.79	7.42	9.18	5.76	2.23
search range	2.5 × 10^5 → 7.5 × 10^7	6.5 × 10^5 → 9.6 × 10^7	1.5 × 10^6 → 8.3 × 10^{10}	1.0 × 10^7 → 9.0 × 10^{11}	2.0 × 10^{-10} → 8.8 × 10^{-13}	

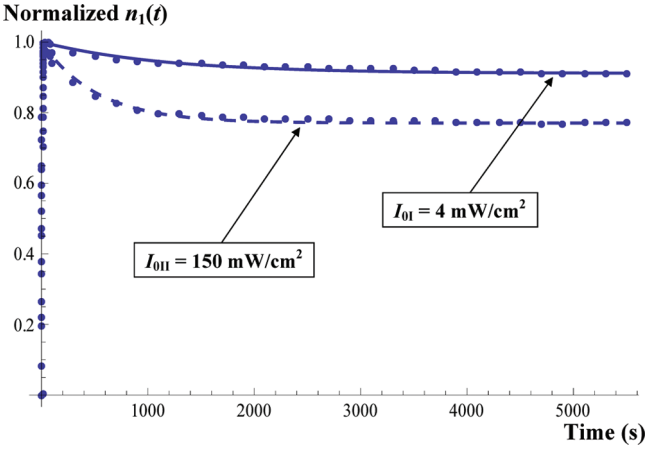

Figure 8. Fit to the experimental data (dots) of decay curves of refractive index modulation for exposing intensities: I_{0I} = 4 mW/cm^2 (solid curve) and I_{0II} = 150 mW/cm^2 (dashed curve).

Δn_1 is the maximum amplitude of the index variation. α_P represents the grating decay constant, which can be expressed as, $\alpha_P = D_p K^2$,[17] where D_p (cm^2/s) is the average diffusion coefficient of all polymer chains, which is assumed to be constant throughout the medium. Applying the nonlinear fitting algorithm, eq 23 is used to fit the normalized experimental decay curves of $n_1(t)$, α_P (hence D_p) can then be determined. The results are presented in Figure 8 for exposing intensities I_{0I} = 4 mW/cm^2 and I_{0II} = 150 mW/cm^2 respectively.

It is clear to see that, for the high intensity case, the refractive index modulation decays much more rapidly and significantly than in the low intensity case. This would appear to confirm that the polymer chains are greatly shortened and thus more mobile, as quantified by a faster polymer diffusion coefficient estimated to be, $D_p(I_{0II}) = 3.55 \times 10^{-13}$ cm^2/s, rather than $D_p(I_{0I}) = 1.6 \times 10^{-15}$ cm^2/s. The corresponding MSE values are also provided for each fit, where MSE (I_{0I}) = 7.79×10^{-9} and MSE (I_{0II}) = 9.21×10^{-9}.

5. Conclusion and Discussion

In this article, starting from a thorough review of the major photochemical reactions and material transportations effects which take place during and postholographic recordings, a more complete and physical representation of material behavior is obtained, which fully incorporates the developed photoinitiation model into the nonlocal photopolymerization driven diffusion (NPDD) model. The resulting coupled differential rate equations, which govern the spatial and temporal concentration variations of each associated chemical species, are presented. This resulting model is significantly improve by the inclucions of the following: (1) a more exact description of photoinitiation; (2) nonsteady state kinetics with nonlocal chain growth, which leads to a more accurate estimation for the concentrations of radicals [$\mathbf{R}^\bullet$, $\mathbf{M}^\bullet$] and polymer [**P**], (including their generations and removals), thus permitting the estimation of the polymerization rate, $\mathbf{R}_p$; (3) multiple termination and inhibition effects.

The predictions made using the model developed, i.e., eqs 2−7, 10-12, 14, 17, and 18, are examined by performing simulation works. These predictions are made under particular conditions of high intensity exposures. The spatial concentration distributions of the most significant chemical species, the different polymerization rates, and the primary termination effects are then illustrated [i.e., Figures 1−4], along with detailed comparisons and analyses for a range of high exposure intensities. Special attention is given to the observed variations of the substantial primary termination effects, which are in comparisons with the bimolecular termination effects, in order to obtain physical insights and assist in determining the corresponding kinetic parameters.

The model is then validated by performing a sequence of experimental work, where several significant achievements have been made, including:

(a) The comparisons of transmission curves for single- (uniform) and double-beam (holographic) exposures. The results are then discussed and it is noted that the differences indicate different absorption behaviors. These results also provide a deeper understanding of how photon absorption under different illuminations leads to the radical productions during the photopolymerization processes.

(b) The performances of refractive index modulations for a range of high exposure intensities are examined. The reduction of the saturation value, n_{1sat}, with increasing exposure intensity is then further explained, and seen to correlate with the progressively amplified primary termination effects. Significantly, combining these results with our detailed explanation of the multiple termination mechanisms, a more physical value of the primary termination rate constant, k_{tp}, is then determined by performing best fits to the experimental results presented in Figure 6.

(c) As indicated, because of the high exposure intensity, significant inhibition periods, t_i, are not observable in Figure 6. However, a detailed explanation is provided in terms of rapid consumption of the inhibitors due to the high intensity exposures.

(d) The decay of the recorded gratings (i.e., for uncrosslinked polymer chains) index is observed over significant postexposure time. Comparisons are also carried out between the results for both low and high exposure intensities. These clearly show a difference between the polymer chain lengths (molecular weights) formed, in terms of the observed polymer diffusion rates.

(e) Finally, based on the theoretical analyses and discussions, and on the fits of the resulting model to the experimental results, key kinetic parameter values are then extracted. These estimated values lie in the reasonable and physical ranges, as indicated in the literature.[7−9,11−20,23,24]

While significant progress is reported in this paper, further work remains to be done. A more inclusive study of various types of photosensitizer in photopolymer materials[4,10,22,27,32] must be carried out, characterizing different dye excitations and subsequently determining the radicals generation. Time varying viscosity, and associated shrinkage and swelling effects[7,9,12,30,33] involving volume variations in the layer, must also be investigated. Such studies will allow further generalization with a more rigorous and comprehensive modeling of free radical photopolymerization processes. The availability of reliable models facilitates the optimization of material compositions for particular applications.

Acknowledgment. We acknowledge the financial support of Enterprise Ireland, Science Foundation Ireland, and the Irish Research Council for Science Engineering, and Technology under the National Development Plan.

References and Notes

(1) Hayashida, N.; Kosuda, A.; Yoshinari, J. *Jpn. J. Appl. Phys.* **2008**, *47*, 5895–5899.
(2) Ye, C.; McLeod, R. R. *Opt. Lett.* **2008**, *33*, 2575–2577.
(3) Sato, A.; Scepanovic, M.; Kostuk, R. *Appl. Opt.* **2003**, *42*, 778–784.

(4) Kashin, O.; Tolstik, E.; Matusevich, V.; Kowarschik, R. *J. Opt. Soc. Am. B* **2009**, *26*, 2152–2156.
(5) Liu, S.; Gleeson, M. R.; Sabol, D.; Sheridan, J. T. *J. Appl. Phys.* **2009**, *106*, 104911.
(6) Liu, S.; Gleeson, M. R.; Guo, J.; Sheridan, J. T. *Appl. Phys. B: Laser Opt.* **2010**, *100*, 559–569.
(7) Gleeson, M. R.; Sheridan, J. T. *J. Opt. Soc. Am. B* **2009**, *26*, 1736–1745.
(8) Gleeson, M. R.; Liu, S.; McLeod, R. R.; Sheridan, J. T. *J. Opt. Soc. Am. B* **2009**, *26*, 1746–1754.
(9) Gleeson, M. R.; Liu, S.; Guo, J.; Sheridan, J. T. *J. Opt. Soc. Am. B* **2010**, *27*, 1804–1812.
(10) Liu, S.; Gleeson, M. R.; Sheridan, J. T. *J. Opt. Soc. Am. B* **2009**, *26*, 528–536.
(11) Odian, G. *Principles of Polymerization*; Wiley: New York, 1991.
(12) Goodner, M. D.; Bowman, C. N. *Macromolecules* **1999**, *32*, 6552–6559.
(13) Tobita, H. *Macromolecules* **1996**, *29*, 3073–3080.
(14) Yan, D.; Zhang, M.; Schweer, J. *Macromolecules* **1996**, *29*, 3793–3799.
(15) Carre, C.; Lougnot, D. J.; Fouassier, J. P. *Macromolecules* **1989**, *22*, 791–799.
(16) Gleeson, M. R.; Kelly, J. V.; Sabol, D.; Close, C. E.; Liu, S.; Sheridan, J. T. *J. Appl. Phys.* **2007**, *102*, 023108.
(17) Gleeson, M. R.; Sabol, D.; Liu, S.; Close, C. E.; Kelly, J. V.; Sheridan, J. T. *J. Opt. Soc. Am. B* **2008**, *25*, 396–406.
(18) Kwon, J. H.; Hwang, H. C.; Woo, K. C. *J. Opt. Soc. Am. B* **1999**, *16*, 1651–1657.
(19) Bamford, C. H.; Jenkins, A. D.; Johnston, R. *Trans. Faraday Soc.* **1959**, *55*, 1451–1460.
(20) Sheridan, J. T.; Lawrence, J. R. *J. Opt. Soc. Am. B* **2000**, *17*, 1108–1114.
(21) Mahabadi, H. K. *Macromolecules* **1985**, *18*, 1319–1324.
(22) Zhao, G. H.; Mouroulis, P. *J. Mod. Opt.* **1994**, *41*, 1929–1939.
(23) Sheridan, J. T.; Gleeson, M. R.; Close, C. E.; Kelly, J. V. *J. Nanosci. Nanotechnol.* **2007**, *7*, 232–242.
(24) Faldi, A.; Tirrell, M.; Lodge, T. P. *Macromolecules* **1994**, *27*, 4176–4183.
(25) Gleeson, M. R.; Liu, S.; Sheridan, J. T. *J. Mater. Sci.* **2009**, *44*, 6090–6099.
(26) Gleeson, M. R.; Kelly, J. V.; O'Neill, F. T.; Sheridan, J. T. *Appl. Opt.* **2005**, *44*, 5475–5482.
(27) Sabol, D.; Gleeson, M. R.; Liu, S.; Sheridan, J. T. *J. Appl. Phys.* **2010**, *107*, 053113.
(28) Wang, J.; Sun, X. D.; Luo, S. H.; Jiang, Y. Y.; Meng, Q. X. *Chin. Phys. B* **2009**, *18*, 4327–4332.
(29) Guo, J.; Liu, S.; Gleeson, M. R.; Sheridan, J. T. *J. Opt. Eng.* **2010**, in press.
(30) Kogelnik, H. *Bell Syst. Tech. J.* **1969**, *48*, 2909–2945.
(31) Kelly, J. V.; Gleeson, M. R.; Close, C. E.; O'Neill, F. T.; Sheridan, J. T.; Gallego, S.; Neipp, C. *Opt. Exp.* **2005**, *13*, 6990–7004.
(32) Pu, H.; Yin, D.; Gao, B.; Gao, H.; Dai, H.; Liu, J. *J. Appl. Phys.* **2009**, *106*, 083111.
(33) Chen, J. H.; Yang, C. T.; Cheng, C. C.; Hsu, M. F.; Jeng, T. R. *IEEE Trans. Mag.* **2009**, *45*, 2252–2255.